JACS
JOURNAL OF THE AMERICAN CHEMICAL SOCIETY
Article
pubs.acs.org/JACS

Optical Properties and Electronic Energy Relaxation of Metallic $Au_{144}(SR)_{60}$ Nanoclusters

Chongyue Yi,[†] Marcus A. Tofanelli,[‡] Christopher J. Ackerson,[‡] and Kenneth L. Knappenberger, Jr.*[,†]

[†]Department of Chemistry and Biochemistry, Florida State University, Tallahassee, Florida 32306, United States
[‡]Department of Chemistry, Colorado State University, Fort Collins, Colorado 80521, United States

Supporting Information

ABSTRACT: Electronic energy relaxation of $Au_{144}(SR)_{60}^{q}$ ligand-protected nanoclusters, where SR = SC_6H_{13} and q = −1, 0, +1, and +2, was examined using femtosecond time-resolved transient absorption spectroscopy. The observed differential transient spectra contained three distinct components: (1) transient bleaches at 525 and 600 nm, (2) broad visible excited-state absorption (ESA), and (3) stimulated emission (SE) at 670 nm. The bleach recovery kinetics depended upon the excitation pulse energy and were thus attributed to electron−phonon coupling typical of metallic nanostructures. The prominent bleach at 525 nm was assigned to a core-localized plasmon resonance (CLPR). ESA decay kinetics were oxidation-state dependent and could be described using a metal-sphere charging model. The dynamics, emission energy, and intensity of the SE peak exhibited dielectric-dependent responses indicative of Superatom charge transfer states. On the basis of these data, the $Au_{144}(SR)_{60}$ system is the smallest-known nanocluster to exhibit quantifiable electron dynamics and optical properties characteristic of metals.

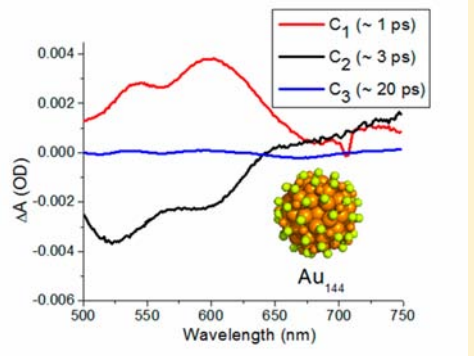

INTRODUCTION

Metallic nanostructures represent a promising class of nanomaterials for catalysis, medical diagnostics, therapeutics, and the utilization of electromagnetic energy.[1−6] Many of these opportunities depend on the unique optical and electronic properties exhibited by metals confined to nanoscale dimensions. For colloidal nanoparticles, these properties change dramatically over the nanometer length scale, evolving from subnanometer, quantum-confined nanoclusters with discrete electronic orbitals and HOMO−LUMO energy gaps to the collective properties of plasmon-supporting nanoparticles (>2 nm). Although significant progress has been made using Superatom models to describe the electronic structure of smaller nanoclusters,[7−15] and classical approaches accurately account for the optical and electronic characteristics of larger nanoparticles,[16,17] the properties—including the onset of metallic behavior—of intermediate (∼1.5 nm) nanometals are poorly understood. Monolayer-protected gold nanoclusters (MPCs) are an emerging class of nanomaterials, which can be examined in an attempt to bridge the gap in understanding the evolution from molecular to bulk metal behavior. Much like gas-phase clusters, specific "magic" sizes of MPCs can be isolated based on a combination of electronic and geometric shell closings.[7−15,18−20] Moreover, synthetic and electrochemical methods exist for tailoring the optical, electronic, and capacitive properties of these materials.[3,18,21−25]

The $Au_{144}(SR)_{60}$ MPC, where SR is SC_6H_{13}, nanocluster is especially well-suited for studying the properties of 1−2 nm nanometals. Widely accepted DFT models that are consistent with structural data posit a core−shell structure that contains a polyhedral 114-atom gold core, which is protected by 30 RS-Au-RS "staple" moieties in the outer shell.[18,26] The core has three concentric shells of 12, (42), and 60 symmetrically equivalent atoms, yielding a total core diameter of 1.5 nm, with a total inorganic diameter of 1.8 nm including the RS-Au-RS units.[18,27] The first evidence of the metal-like behavior for Au_{144} was obtained from electrochemical and tunneling microscopy measurements that indicated that these nanoclusters could accommodate classical double-layer charging,[21] with up to 15 discrete charge states resolvable for this MPC.[28] These results are supported by recent infrared absorption measurements and electronic-structure calculations that suggest Au_{144} nanoclusters are gapless.[25] A 20-meV energy gap was detected in the HOMO−LUMO energy region, but this effect arose from spectroscopic selection rules.[25] Simulated optical spectra for $Au_{144}(SH)_{60}$ included two peaks at 540 and 600 nm, for which the electron densities are localized to the 114-atom core.[18,29] Taken together, these results suggest $Au_{144}(SR)_{60}$ is an ideal prototype for studying the onset of *metallic* electronic relaxation and optical properties, including emergent plasmon phenomena.

Femtosecond time-resolved differential extinction spectroscopy is a reliable experimental diagnostic for quantifying the optical and electronic properties of metal nanostructures.[30−41] Excitation of metals by short-pulse lasers generates a non-

Received: October 3, 2013
Published: November 6, 2013

   dx.doi.org/10.1021/ja409998j | J. Am. Chem. Soc. 2013, 135, 18222−18228

equilibrium electron gas, which subsequently cools through coupling with the phonon bath of the metal lattice over a picosecond time scale.[29] Formation of the hot electron gas results in a transient bleach in the differential extinction spectra at the plasmon resonance wavelength of the nanoparticle. The dynamics of the approximately picosecond electron−phonon equilibration can be recorded by monitoring the time-dependent recovery of the plasmon bleach. For metals, these electron cooling rates depend directly on the excitation pulse energy.[30]

Here, we present the results of a study of femtosecond time-resolved transient extinction measurements of $Au_{144}(SC_6H_{13})_{60}$ manipulated by bulk electrolysis into 4 different oxidation states, q (q = −1, 0, +1, +2). We provide the first direct experimental evidence of MPCs displaying electronic energy relaxation characteristic of metallic nanostructures, with a quantifiable electron−phonon coupling constant. Also, transient difference spectra included discrete peaks at visible wavelengths, consistent with a collective resonance of the free electrons, which we described as a core-localized plasmon resonance (CLPR). Although significant contributions from Superatom orbitals were required to account fully for the observed relaxation dynamics, the 144-gold-atom nanocluster is, to date, the smallest cluster known to exhibit metallic electronic-energy relaxation dynamics and optical properties.

RESULTS AND DISCUSSION

For all time- and wavelength-resolved transient extinction measurements, $Au_{144}(SR)_{60}$ nanoclusters were excited using the 400-nm second harmonic of an amplified Ti:sapphire laser, and the time domain relaxation dynamics were recorded using a temporally delayed broad-bandwidth visible continuum pulse. The experimental setup has been described previoulsy;[42] pertinent details are provided as Supporting Information. The 400-nm excitation was resonant with multiple nanocluster states that included contributions from the ligand shell and the gold interband transition.[18] Figure 1 portrays typical transient differential extinction spectra for nanoclusters in the q = −1 (a), 0 (b), +1 (c), and +2 (d) oxidation states recorded at a pump−probe time delay of 0.8 ps. For all oxidation states, the transient spectra included three distinct components: (i) ground-state bleach at short wavelengths, (ii) broad excited-state absorption (ESA) that spanned most of the visible spectrum, and (iii) transient induced transparency at 670 nm, which we attributed to stimulated emission. Analysis of the time-domain response was complicated by the spectral overlap of the three components described above, which resulted primarily from the broad ESA peak. Although the general features of the transient spectra were consistent for all four oxidation states, the magnitude of the stimulated emission decreased with increasing oxidation state.

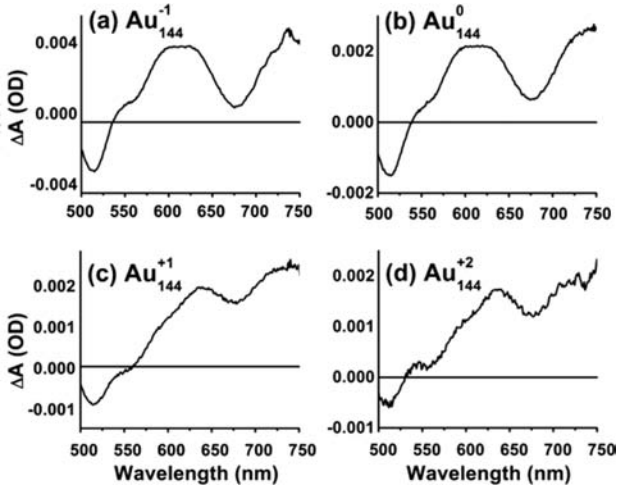

Figure 1. Differential transient extinction spectra obtained for $Au_{144}(SR)_{60}$ MPCs in the (a) q = −1, (b) q = 0, (c) q = +1, and (d) q = +2 oxidations states. Transient spectra were recorded at a pump−probe time delay of 0.8 ps, following excitation by 90-fs pulses of 400-nm light.

To study the dynamics of electronic relaxation, the transient data were analyzed using global analysis and singular value decomposition methods.[43] In this way, the contribution of each component to the time-dependent decay of the transient data could be resolved. Figure 2 portrays the results from global analysis. For the q = 0 and −1 oxidation states, the best result included three components, which distinguished ground-state bleaching, excited-state absorption and stimulated emission. The stimulated emission component is amplified in the inset of Figure 2a. In contrast, only two components were included in the global analysis results for the q = +1 and +2 oxidation states (Figure 2b), which corresponded to ground-state bleaching and excited-state absorption. This result was not surprising based

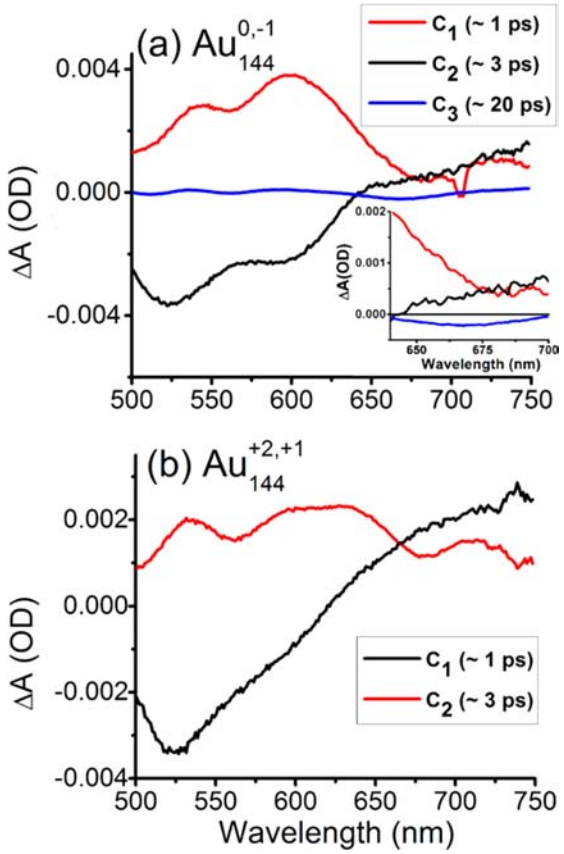

Figure 2. (a) Global analysis results obtained from the differential transient extinction spectra typical for $Au_{144}(SR)_{60}$ MPCs in the q = −1 and q = 0. The spectra included three distinct components. (b) Global analysis results obtained from the differential transient extinction spectra typical for $Au_{144}(SR)_{60}$ MPCs in the q = +1, and q = +2 oxidations states. The spectra included two distinguishable components.

dx.doi.org/10.1021/ja409998j | J. Am. Chem. Soc. 2013, 135, 18222−18228

on the relatively weak stimulated emission observed for nanoclusters in positive oxidation states. Temporal analysis of the three components yielded characteristic time constants of (i) ~1 ps, (ii) ~3 ps, and (iii) ~20 ps. These three components, which provided direct experimental evidence for metallic electron energy relaxation, as well as relaxation via Superatom states, will be discussed separately.

Component 1: Ground-State Bleaching. Component one contributes negative amplitude to the transient difference spectra with an onset of approximately 630 nm, reminiscent of the well-known LSPR bleach exhibited by larger colloidal gold nanoparticles. This bleach component contributed two peaks with maxima at 525 and 600 nm, consistent with electronic structure calculations.[18] The intensity of the 600-nm component was most significant for nanoclusters with q = 0, −1. To determine the nature of electronic energy relaxation in the Au_{144} nanoclusters, the time dependence of the component-1 bleach recovery was monitored. Time-domain data obtained after electronic excitation of the $Au_{144}(0)$ nanocluster using a range of excitation pulse energies are shown in Figure 3a. These time-dependent traces were generated using the magnitude of the 525-nm transient bleach signal as a function of time after nanocluster excitation. For this sample, the pump laser power was varied from 300 to 800 nJ per pulse, with larger pulse energies resulting in longer relaxation times. The experimental time-domain data were fit using an exponential decay function. The instrument response function was deconvoluted to the Gaussian pump and probe laser pulses using a program written in house that relies on an iterative least-squares approach.[42]

To examine more carefully the excitation pulse energy dependence of the data in Figure 3a, the resulting time constants were plotted as a function of laser pulse energy in Figure 3b. Although Figure 3b portrays only the data obtained for the neutral $Au_{144}(SR)_{60}$ system, the relaxation time constants for all four nanocluster oxidation states were linearly dependent on excitation pulse energy; the complete data set is provided as Supporting Information. Linear power-dependent data are a characteristic feature of electron cooling in metallic nanostructures and are accurately described using the two-temperature model.[44,45] The use of pulsed lasers to excite metals results in the formation of a nonequilibrium electron gas. In the two-temperature model, the electron gas and the metal lattice are treated as two coupled subsystems at different temperatures; upon impulsive excitation, the temperature of the electron gas is determined by the laser pulse energy, whereas the lattice remains at room temperature. The extent of electron−phonon coupling determines the rate of energy flow from the electron gas to the lattice. The two-temperature model can be described using eqs 1 and 2:[44,45]

$$C_e(T_e)(\delta T_e/\delta t) = -G(T_e - T_l) \quad \text{and}$$
$$C_l(\delta T_l/\delta t) = G(T_e - T_l) \tag{1}$$

$$C_e(T_e) = \gamma T_e \tag{2}$$

where T_e and T_l are the respective temperatures of the electron gas and the lattice, and C_e and C_l are the electron and lattice heat capacities. The coupling of T_e and T_l is quantified by the electron−phonon coupling constant, G. The linear dependence of the relaxation time constant on the excitation pulse energy results from the direct dependence of C_e on T_e, as shown in eq 2 where γ = 66 J m^{-3} K^{-2} for gold.[30]

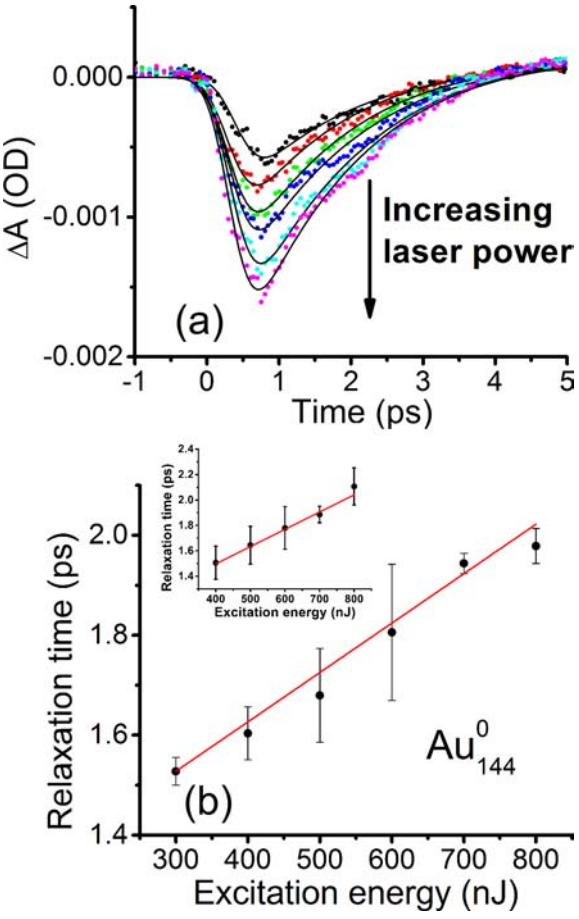

Figure 3. (a) Bleach recovery kinetics observed for the 525-nm bleach component (for the neutral species) for a series of laser excitation pulse energies. The data were fit to an exponential decay function. Longer relaxation time constants were obtained for higher laser pulse energies. (b) Relaxation time constants determined for the 525-nm (component 1) bleach recovery when different laser excitation pulse energies were used to excite the sample. The two-temperature model was used to determine the nanocluster room-temperature electron−phonon coupling time constant from the y-intercept of the linear fit. Data obtained from $Au_{144}(SR)_{60}$ nanoclusters provided good agreement with data for citrate-stabilized solid gold nanospheres (inset, panel b).

Hence, the pulse-energy dependence of the relaxation time constants could be used to quantify the electron−phonon coupling constants observed for the Au_{144} nanoclusters. First, the room-temperature electron−phonon coupling time constant was determined for the Au_{144} nanoclusters by applying a linear fit to the data in Figure 3b and extrapolating to zero laser pulse energy. The room-temperature time constant obtained in this manner was then converted to the nanocluster electron−phonon coupling constant using eq 3:[30]

$$\tau_0 = \gamma T_0/G \tag{3}$$

Analysis of all four nanoclusters yielded an average electron−phonon coupling constant of $G = (1.68 \pm 0.15) \times 10^{16}$ W m^{3-} K^{-1}. This value agreed well with the reported value of ~2 × 10^{16} W m^{3-} K^{-1} for larger citrate-stabilized gold nanoparticles;[30] using the same laser system as in the current study, we recently obtained $G = 1.85 \times 10^{16}$ W m^{3-} K^{-1} for solid gold nanospheres ranging from 20 to 83 nm in diameter.[42] Therefore, the bleach-recovery results for $Au_{144}(SR)_{60}$ nano-

dx.doi.org/10.1021/ja409998j | J. Am. Chem. Soc. 2013, 135, 18222−18228

clusters agreed well with electron−lattice equilibration, which we attribute to interband excitation of the 114-atom gold core of the nanocluster. The small differences in the G values of the nanoclusters and nanoparticles could arise from the dispersing medium and capping ligands; the nanoclusters are stabilized by thiols whereas the large nanoparticles are capped using citrate. Taken together, the transient bleach at 525 nm and the electron cooling dynamics suggested that the Au_{144} nanoclusters exhibited properties characteristic of larger plasmonic noble metal nanoparticles. Although transient extinction measurements have been performed on other ligand-protected gold nanoclusters,[46−50] these data provide the first experimental evidence of quantifiable electron−phonon coupling that is characteristic of a metal nanostructure. Previous experiments carried out on Au_{55} revealed a rapid energy relaxation process occurring on a picosecond time scale, but an electron−phonon coupling constant could not be determined for those clusters.[34]

The electronic relaxation dynamics of the Au_{144} nanoclusters were consistent with electronic structure calculations[25] as well as electrochemical measurements[21] that predict a vanishing energy gap separating the HOMO and LUMO levels and the onset of metallic behavior. The gap closing also results in a high density of states in the HOMO−LUMO region, leading to efficient electrical charging.[21] The capacitive properties of $Au_{144}(SR)_{60}$ nanoclusters can be described using a metallic-sphere model. Nonlinear absorption measurements provide further evidence of metallic behavior for $Au_{144}(SR)_{60}$ nanoclusters.[51] Recent electronic structure calculations indicate that optical excitation of $Au_{144}(SR)_{60}$ nanoclusters results in a collective resonance that is localized to the nanocluster core.[29] This collective resonance likely gives rise to the transient bleach observed at 525 nm in the differential extinction spectra following 400-nm excitation of the $Au_{144}(SR)_{60}$ interband transition. Because this resonance is confined to the interior core of the core−shell nanoparticle, we distinguish it from the localized surface plasmon resonances (LSPR) of colloidal nanoparticles by calling it a core-localized plasmon resonance (CLPR). To our knowledge, these transient data provide the first experimental observation of a prominent CLPR transition. Moreover, the 144-atom nanocluster is the smallest gold system for which a plasmon resonance has been verified and characteristic *metallic* electron cooling has been quantified.

Component 2: Excited-State Absorption. Further direct evidence of the metallic behavior of Au_{144} nanoclusters was obtained from the oxidation state-dependent kinetics of component two (excited state absorption). In addition to exciting the interband transition, the 400-nm pump pulse is also resonant with excited states that include mixed contributions from Au(sp) and ligand orbitals.[18,25] For smaller nanoclusters, these Superatom states relax by rapid internal conversion to the HOMO level and subsequent charge transfer to states localized on the "RS-Au-RS" staple unit (outer shell).[46,47] For the metallic $Au_{144}(SR)_{60}$, the HOMO consists of a manifold of electronic states, which account for the capacitive properties of the nanocluster. Consistent with the behavior of metal spheres, charging of $Au_{144}(SR)_{60}$ nanoclusters induces small energy gaps that separate the states located near the HOMO.[18,21] In order to study the oxidation-state dependence of states near the HOMO, we analyzed the relaxation time constant of component 2, which reports on electron thermalization near the HOMO. The time-dependent magnitudes of the difference absorption signal obtained for nanoclusters in q = 0 and q = +2 oxidation states are compared in the log−linear plot in Figure 4a. The q = +2 nanocluster clearly exhibited a longer relaxation time constant than the neutral species. The component-2 time

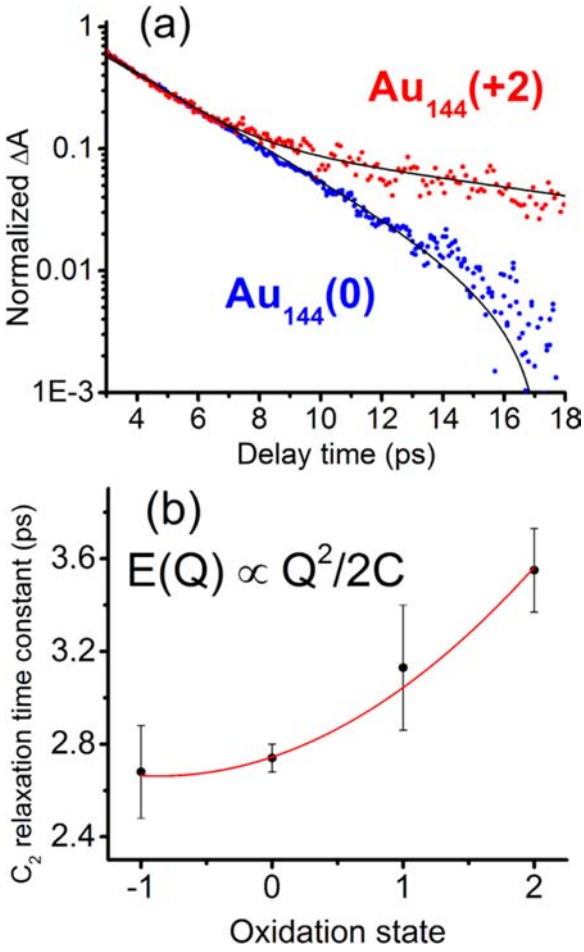

Figure 4. (a) Comparison of the component 2 principle kinetics obtained for $Au_{144}(SR)_{60}$ in the q = 0 (blue) and q = +2 (red) oxidation states. The black lines represent fits to the data obtained using an exponential decay function. The time-dependent data clearly reflected slower relaxation rates for the nanocluster with a higher oxidation state. (b) Component 2 (C_2) relaxation time constant plotted as a function of nanocluster oxidation state. The red line portrays the quadratic fit that was applied to the data. The average and standard deviation was obtained from statistical analysis of the results from several experiments.

constants obtained for all four nanoclusters are summarized in Table 1 and Figure 4b. The best fit to the data in Figure 4b

Table 1. Summary of Component 2 Fitting Results

cluster	t_2 (ps)
$Au_{144}(SR)_{60}^{-1}$	2.68 ± 0.20
$Au_{144}(SR)_{60}^{0}$	2.74 ± 0.06
$Au_{144}(SR)_{60}^{+1}$	3.13 ± 0.27
$Au_{144}(SR)_{60}^{+2}$	3.55 ± 0.18

indicated that the component-2 relaxation time constant exhibited a quadratic dependence on the oxidation state of the nanocluster, with more oxidized clusters displaying longer time constants.

The quadratic dependence noted in the data in Figure 4b can be explained by considering the charging behavior of metal

dx.doi.org/10.1021/ja409998j | J. Am. Chem. Soc. 2013, 135, 18222−18228

spheres. In this model, the energy required to add a charge to a metallic sphere increases quadratically with charge state [$E(Q) \propto Q^2/2C$, where C is capacitance].[21] Indeed, electronic structure calculations for the Au_{144} nanoclusters examined here reveal an energy gap that increases quadratically with increasing charge state.[18] Therefore, the oxidation-state dependence of the data in Figure 4b clearly reflected charging effects of the metallic nanoclusters. The time required for an electron to relax from a higher- to a lower-energy state depends upon the size of the energy gap separating the two states; relaxation is fastest for the smallest gap and occurs more slowly for larger gaps.[52] Considering electronic relaxation through the manifold of states near the HOMO level, the larger time constants obtained for higher charge states of the Au_{144} nanocluster resulted from the larger energy gap separating the states in this region.

Taken together, the excitation-pulse-energy-dependent electron−phonon equilibration (component 1) and electron thermalization (component 2) provided strong, direct evidence of the metallic properties of the Au_{144} nanocluster. To our knowledge, this study, which combined ultrafast laser spectroscopy with controlled electrochemical preparation of nanocluster charge states, provides the first experimental evidence of metallic electron relaxation dynamics for ultrasmall, ligand-protected nanoclusters.

Component 3: Stimulated Emission. The third component of the transient spectra resulted from transient induced transparency at 670 nm, which we attributed to stimulated emission. The magnitude of the component 3 signal increased concomitantly with the probe energy, and the peak energy, amplitude, and width all exhibited time-dependent behaviors. These factors implied that the spectral feature at 670 nm resulted from stimulated emission rather than saturated ground-state absorption.[53] As portrayed by the transient spectra in Figure 1, the relative contribution from stimulated emission was largest for the $q = 0, -1$ nanoclusters, whereas only small contributions were observed for the cationic species. Stimulated emission is often observed in transient extinction spectra of organometallic compounds, and it originates from charge-transfer states.[54] Ligand-to-metal charge transfer processes have been invoked to account for NIR photoluminescence of smaller (Au_{25}) nanoclusters.[55] Nanocluster-to-ligand-shell charge transfer has also been used to reconcile picosecond relaxation dynamics of Au_{25}.[46] However, for Au_{144}, electronic energy relaxation proceeds by rapid thermalization of a manifold of states with an electron gap of approximately 20 meV. On the basis of energy conserving arguments, this relaxation process should preclude electron transfer from the nanocluster to the ligand shell. One possible explanation to account for component three dynamics is that the time-dependent stimulated emission signal tracks electronic energy relaxation of charge-transfer Superatomic orbitals with significant ligand character that are excited independently of the nanocluster core. On the basis of electronic structure calculations, 400-nm pumping of $Au_{144}(SR)_{60}$ excites both the interband transition and ligand states.[25]

To examine whether component three resulted from stimulated emission mediated by charge-transfer Superatom states, we analyzed the integrated intensities (Figure 5a; blue) and emission energy (Figure 5a; red) of the stimulated-emission signal component in a series of solvents with dielectric constants ranging from 2.4 to 9.1. The data in Figure 5a were generated by analyzing the stimulated-emission peak for the

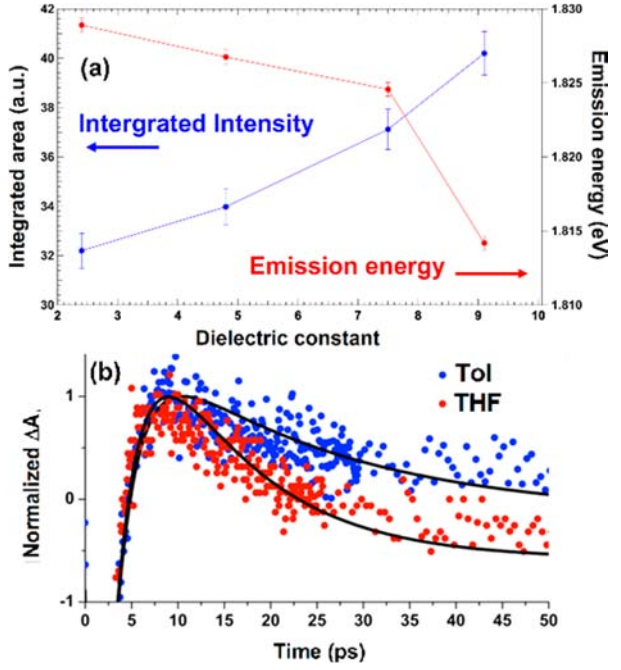

Figure 5. Component 3 (stimulated emission) solvent dependence obtained for the neutral $Au_{144}(SR)_{60}$ nanocluster. (a) Integrated intensity (blue) and emission energy (red) of the stimulated emission peak plotted versus solvent dielectric constant. All data were obtained from analysis of the stimulated emission peak recorded at a pump−probe delay of 1 ps, following excitation using 400-nm light. The average and standard deviations for the integrated intensities and emission energies were obtained from statistical analysis of the results from several experiments. (b) Normalized, and inverted, time-dependent amplitude of the stimulated emission signal (blue, toluene; red, tetrahydrofuran). The black line represents a fit using a biexponential function that included an initial growth and subsequent decay components. The energy, intensity and time-dependence of the stimulated emission peaks were all sensitive to the dispersing solvent.

neutral nanocluster obtained at a pump−probe time delay of 1 ps. Upon increasing the solvent dielectric constant from 2.4 to 9.1, we observed an increase in stimulated emission intensity. This observation was consistent with expectations because the larger dielectric constant stabilized the charge-transfer state, yielding greater stimulated-emission intensity. The shift to lower energies with increasing dielectric constant was also expected because of charge-transfer stabilization. In fact, the temporal response provided evidence that the charge-transfer states relaxed into a lower-energy stabilized-charge-transfer state (Figure 5b). As the time-dependent stimulated emission data in Figure 5b illustrate, the magnitude of the induced transparency increased exponentially during the first few picoseconds and then subsequently decayed with an apparent time constant of 18 ± 2 ps (neutral $Au_{144}(SR)_{60}$ dispersed in toluene; blue data). Upon increasing the solvent polarity (THF; $\varepsilon = 7.5$),[56] the relaxation time constant decreased to 8 ± 2 ps. These data indicated that relaxation from an initial charge-transfer state into a stabilized configuration was facilitated when the nanoclusters were dispersed in solvents with large dielectric constants. We also analyzed the time-dependent stimulated-emission energy and bandwidth (Figure S3). As expected, the bandwidth increased at longer pump−probe time delays owing to thermalization processes.

Electronic energy relaxation of $Au_{144}(SR)_{60}$ nanoclusters proceeds via several mechanisms. Systematic analysis of the

dx.doi.org/10.1021/ja409998j | J. Am. Chem. Soc. 2013, 135, 18222−18228

multicomponent transient extinction spectra allowed for elucidation of these processes. Two of these components (C_1 and C_2) exhibited the characteristic features of electronic energy relaxation for metal nanostructures, thereby providing direct evidence of the metallic behavior of the ligand-protected Au_{144} system. However, analysis of component 3, which showed signatures of charge-transfer states, suggested that Superatom concepts are still needed for providing a complete description of the electron dynamics of monolayer-protected nanoclusters with diameters of approximately 1.8 nm.

CONCLUSIONS

We have presented the first systematic study of electronic energy relaxation of $Au_{144}(SR)_{60}$ nanoclusters using a comprehensive range of oxidation states. Our ultrafast transient extinction data showed direct evidence of the metallic properties of this nanocluster. To our knowledge, the $Au_{144}(SR)_{60}$ species is the smallest gold nanoparticle to exhibit quantifiable metallic behavior. The transient-difference spectra obtained for $Au_{144}(SR)_{60}$ also provided compelling experimental evidence for collective optical excitations that localize electron density to the interior core of the nanocluster. We designate these optical transitions as core-localized plasmon resonances. The potential impacts of metal nanostructure optical, thermal, and electrical properties are far reaching, with applications including applied spectroscopy, solar-to-electric energy conversion, medical imaging and therapeutics, and nonlinear optical technologies based on negative index metamaterials. Clearly, gold nanoparticles with diameters of approximately 1.8 nm are important nanomaterials for developing a predictive understanding of the transition from molecular to bulk-like properties.

ASSOCIATED CONTENT

Supporting Information

Synthetic protocol, experiment setup, absorption spectrum of Au_{144} and electron phonon coupling time constants of clusters with different oxidation states. This material is available free of charge via the Internet at http://pubs.acs.org.

AUTHOR INFORMATION

Corresponding Author

klk@chem.fsu.edu

Notes

The authors declare no competing financial interest.

ACKNOWLEDGMENTS

This work has been supported by a National Science Foundation (NSF) award to K.L.K., grant number CHE-1150249. C.J.A. and M.A.T. acknowledge Colorado State University for support. The authors acknowledge Hannu Häkkinen for helpful discussions.

REFERENCES

(1) Valden, M.; Lai, X.; Goodman, D. W. *Science* **1998**, *281*, 1647–1650.
(2) Hirsch, L. R.; Stafford, R. J.; Bankson, J. A.; Sershen, S. R.; Rivera, B.; Price, R. E.; Hazle, J. D.; Halas, N. J.; West, J. L. *Proc. Natl. Acad. Sci. U.S.A.* **2003**, *100*, 13540–13554.
(3) McCoy, R. S.; Choi, S.; Collins, G.; Ackerson, B. J.; Ackerson, C. J. *ACS Nano* **2013**, *7*, 2610–2616.
(4) Knappenberger, K. L., Jr.; Dowgiallo, A. M.; Chandra, M.; Jarrett, J. W. *J. Phys. Chem. Lett.* **2013**, *4*, 1109–1119.
(5) Daniel, M.-C.; Astruc, D. *Chem. Rev.* **2004**, *104*, 293–346.
(6) Sardar, R.; Funston, A.; Mulvaney, P.; Murray, R. *Langmuir* **2009**, *24*, 13840–13851.
(7) Aikens, C. M. *J. Phys. Chem. Lett.* **2010**, *1*, 2594–2599.
(8) Jin, R. *Nanoscale* **2010**, *2*, 343–362.
(9) Price, R. C.; Whetten, R. L. *J. Am. Chem. Soc.* **2005**, *127*, 13750–13751.
(10) Aikens, C. M. *J. Phys. Chem. Lett.* **2011**, *2*, 99–104.
(11) Wyrwas, R. B.; Alvarez, M. M.; Khoury, J. T.; Price, R. C.; Schaaff, T. G.; Whetten, R. L. *Eur. Phys. J. D* **2007**, *43*, 91–95.
(12) Walter, M.; Akola, J.; Lopez-Acevedo, O.; Jadzinsky, P. D.; Calero, G.; Ackerson, C. J.; Whetten, R. L.; Gronbeck, H.; Hakkinen, H. *Proc. Natl. Acad. Sci. U.S.A.* **2008**, *105*, 9157–9162.
(13) Heaven, M. W.; Dass, A.; White, P. S.; Holt, K. M.; Murray, R. W. *J. Am. Chem. Soc.* **2008**, *130*, 3754–3755.
(14) Zhu, M.; Aikens, C. M.; Hollander, F.; Schatz, G.; Jin, R. *J. Am. Chem. Soc.* **2008**, *130*, 5883–5885.
(15) Tofanelli, M. A.; Ackerson, C. *J. Am. Chem. Soc.* **2012**, *134*, 16937–16940.
(16) Mie, G. *Ann. Phys.* **1908**, *330*, 377–445.
(17) Kreibig, U.; Vollmer, M. *Optical Properties of Metal Clusters*; Springer: Berlin-Heidelberg, 1995.
(18) Lopez-Acevedo, O.; Akola, J.; Whetten, R. L.; Grönbeck, H.; Häkkinen, H. *J. Phys. Chem. C* **2009**, *113*, 5035–5038.
(19) Dass, A. *J. Am. Chem. Soc.* **2011**, *133*, 19259–19261.
(20) Knoppe, S.; Boudon, J.; Dolamic, I.; Dass, A.; Burgi, T. *Anal. Chem.* **2011**, *83*, 5056–5061.
(21) Ingram, R. S.; Hostetler, M. J.; Murray, R. W.; Schaaff, T. G.; Khoury, J. T.; Whetten, R. L.; Bigioni, T. P.; Guthrie, D. K.; First, P. N. *J. Am. Chem. Soc.* **1997**, *119*, 9279–9280.
(22) Chaki, N. K.; Negishi, Y.; Tsunoyama, H.; Shichibu, Y.; Tsukuda, T. *J. Am. Chem. Soc.* **2008**, *130*, 8608–8610.
(23) Jadzinsky, P. D.; Calero, G.; Ackerson, C. J.; Bushnell, D. A.; Kornberg, R. D. *Science* **2007**, *318*, 430–433.
(24) Parker, J. F.; Fields-Zinna, C. A.; Murray, R. W. *Acc. Chem. Res.* **2010**, *43*, 1289–1296.
(25) Koivisto, J.; Malola, S.; Kumara, C.; Dass, A.; Hakkinan, H.; Pettersson, M. *J. Phys. Chem. Lett.* **2012**, *3*, 3076–3080.
(26) Wong, O. A.; Heinecke, C. L.; Simone, A. R.; Whetten, R. L.; Ackerson, C. J. *Nanoscale* **2012**, *4*, 4099–4102.
(27) Bahena, D.; Bhattarai, N.; Santiago, U.; Tlahuice, A.; Ponce, A.; Bach, S. B.; Yoon, B.; Whetten, R. L.; Landman, U.; Jose-Yacaman, M. *J. Phys. Chem. Lett.* **2013**, *4*, 975–981.
(28) (a) Hicks, J. F.; Miles, D. T.; Murray, R. W. *J. Am. Chem. Soc.* **2002**, *124*, 13322–13328. (b) Quinn, B. M.; Liljeroth, P.; Ruiz, V.; Laaksonen, T.; Kontturi, K. *J. Am. Chem. Soc.* **2003**, *125*, 6644–6645.
(29) Malola, S.; Lehtovara, L.; Enkovaara, J.; Hakkinan, H. *ACS Nano* **2013**, DOI: 10.1021/nn4046634.
(30) Hartland, G. V. *Phys. Chem. Chem. Phys.* **2004**, *6*, 5263–5274.
(31) Voisin, C.; Del Fatti, N.; Christofilos, D.; Vallee, F. *J. Phys. Chem. B* **2001**, *105*, 2264–2280.
(32) Pelton, M.; Sader, J. E.; Burgin, J.; Liu, M. Z.; Guyot-Sionnest, P.; Gosztola, D. *Nat. Nanotechnol.* **2009**, *4*, 492–495.
(33) Voisin, C.; Del Fatti, N.; Christofilos, D.; Vallee, F. *Appl. Surf. Sci.* **2000**, *164*, 131–139.
(34) Smith, B. A.; Zhang, J. Z.; Giebel, U.; Schmid, G. *Chem. Phys. Lett.* **1997**, *270*, 139–144.
(35) Link, S.; El-Sayed, M. A. *J. Phys. Chem. B* **1999**, *103*, 8410–8426.
(36) Hartland, G. V. J. *Chem. Phys.* **2002**, *116*, 8048–8055.
(37) Averitt, R. D.; Westcott, S. L.; Halas, N. *J. Phys. Rev. B* **1998**, *58*, R10203–10206.
(38) Dowgiallo, A. M.; Knappenberger, K. L., Jr. *J. Am. Chem. Soc.* **2012**, *134*, 19393–19400.
(39) Grant, C. D.; Schwartzberg, A. M.; Yang, Y.; Chen, S.; Zhang, J. Z. *Chem. Phys. Lett.* **2004**, *383*, 31–34.
(40) Guillon, C.; Langot, P.; Del Fatti, N.; Vallee, F.; Kirakosyan, A. S.; Shahbazyan, T. V.; Cardinal, T.; Treguer, M. *Nano Lett.* **2007**, *7*, 138–142.

(41) Dowgiallo, A. M.; Schwartzberg, A. M.; Knappenberger, K. L., Jr. *Nano Lett.* **2011**, *11*, 3258−3262.
(42) Dowgiallo, A. M.; Knappenberger, K. L., Jr. *Phys. Chem. Chem. Phys.* **2011**, *13*, 21585−21592.
(43) Van Stokkum, I. H. M.; Larsen, D. S.; Van Grondelle, R. *Biochim. Biophys. Acta, Bioenerg.* **2004**, *87*, 1858−1872.
(44) Kaganov, M. I.; Lifshitz, I. M.; Tanatarov, L. V. *Sov. Phys.—JETP* **1957**, *4*, 173.
(45) Fujimoto, J. G.; Ippen, E. P.; Bloemberger, N. *Phys. Rev. Lett.* **1984**, *53*, 1837−1840.
(46) Miller, S. A.; Fields-Zinna, C. A.; Murray, R. W.; Moran, A. M. *J. Phys. Chem. Lett.* **2010**, *1*, 1383−1387.
(47) Devadas, M. S.; Kim, J.; Sinn, E.; Lee, D.; Goodson, T. G.; Ramakrishna, G. *J. Phys. Chem. C* **2010**, *114*, 22417−22423.
(48) Qian, H.; Sfeir, M. Y.; Jin, R. *J. Phys. Chem. C* **2010**, *114*, 19935−19940.
(49) Green, T. G.; Knappenberger, K. L., Jr. *Nanoscale* **2012**, *4*, 4111−4118.
(50) Yau, S. H.; Varnavski, O.; Goodson, T. *Acc. Chem. Res.* **2013**, *46*, 1506−1516.
(51) Philip, R.; Chantharasupawong, P.; Qian, H.; Jin, R.; Thomas, J. *Nano Lett.* **2012**, *12*, 4661−4667.
(52) Englman, R.; Jortner, J. *Mol. Phys.* **1970**, *18*, 145−164.
(53) Bingemann, D.; Ernsting, N. P. *J. Chem. Phys.* **1995**, *102*, 2691−2700.
(54) Leung, M. H. M.; Pham, D. T.; Lincoln, S. F.; Kee, T. W. *Phys. Chem. Chem. Phys.* **2012**, *14*, 13580−13587.
(55) Wu, Z.; Jin, R. *Nano Lett.* **2010**, *10*, 2568−2573.
(56) *CRC Handbook of Chemistry and Physics*, 92nd ed.; CRC Press: Boca Raton, FL, 2011−2012; pp 6−242.